Diabatic Ordering of Vibrational Normal Modes in Reaction Valley Studies

ZORAN KONKOLI, DIETER CREMER, ELFI KRAKA

Department of Theoretical Chemistry, University of Göteborg, Kemigården 3, S-41296 Göteborg, Sweden

Received 24 September 1996; accepted 19 January 1997

ABSTRACT: Diabatic ordering of the normal model of a reaction complex along the reaction path has several advantages with regard to adiabatic ordering. The method is based on rotations of the vibrational normal modes at one point, s, of the reaction path to maximize overlap with the vibrational modes at a neighboring point. Global rotations precede the rotations of degenerate modes so that changes in the direction of the reaction path and changes in the force constant matrix, which represent the two major effects for changes in mode ordering, can be separated. Overlap criteria identify resolved and unresolved avoided crossings of normal modes of the same symmetry. Diabatic mode ordering (DMO) can be used to resolve the latter by reducing the step size, thus guaranteeing correct ordering of normal modes in dependence of s. DMO is generally applicable to properties of the reaction complex that depend on s such as normal mode frequencies, orbital energies, the energy of excited states, etc. Additional applications are possible using a generalized reaction path vector, which may describe the change in atom masses, geometrical parameters, and/or the force constant matrix. In this way, the vibrational spectra of isotopomers can be investigated or the vibrational frequencies of different molecules correlated.
 J Comput Chem **18**:1282–1294, 1997

Introduction

Investigations with the reaction path Hamiltonian (RPH) of Miller et al.[1] focus on the reaction path and the associated reaction valley, which is described by 3K-7 normal modes of vibration transverse to the reaction path following mode of a reaction complex with K atoms.[2–5] A key feature of the investigation is the representation of the normal mode frequencies, ω_μ, as a function of the reaction coordinate s in the form $\omega_\mu(s)$.[3,6–11] Depending on the symmetry and electronic structure of the reaction complex one encounters various crossings of the curves $\omega_\mu(s)$ along the reaction path: (a) These can be crossings involving modes of different symmetry, which are allowed. (b) If the crossing modes possess the same symmetry, an avoided crossing will be encountered where the

Correspondence to: D. Cremer

Contract/grant sponsor: Swedish National Science Research Council

 CCC 0192-8651 / 97 / 101282-13

degree of interaction between the modes determines how close the curves $\omega_\mu(s)$ approach at the avoided crossing point before they separate and continue in different directions.

The correct ordering of normal modes before and after a crossing or avoided crossing point is essential for the study of mode–mode coupling that determines the energy dissipation between modes along the reaction path. It is even more important for the characterization of the reaction path curvature, $\kappa(s)$, in terms of normal modes, which is carried out with the help of the normal mode-curvature coupling coefficients, $B_{\mu,s}(s)$.[1–4] Maxima of the curvature $\kappa(s)$ indicate those positions of s at which energy stored in vibrational modes can flow into the translational mode of the reaction complex and, by this, enhance the reaction rate. The normal modes that couple most strongly with the reaction path mode are identified by the coupling coefficients, $B_{\mu,s}(s)$, which can only correctly be determined if the normal modes are correctly ordered throughout the whole reaction path from reactants to products.

In most investigations carried out with the RPH, normal mode ordering is carried out with the help of symmetry because this is a simple means to detect avoided crossing points of $\omega_\mu(s)$. Symmetry criteria also help to correctly label normal modes at allowed crossing points. However, difficulties can arise in the latter case if the reaction complex possesses C_1-symmetry or the symmetry is changed along the reaction path because of one or more bifurcation points.[12] Apart from this, one has to consider numerical problems, which arise from the fact that, depending on the step size used to follow the reaction path, there may be situations where slight deviations from the true path lead to distortions of the reaction complex associated with a lowering of its symmetry and the symmetry of the normal modes. Although these deviations normally do not affect the overall investigation of reaction path and reaction valley, they cause local difficulties in the ordering of normal modes, which can only be resolved by repeating calculations with smaller step size so that deviations from the reaction path are avoided and the symmetry of the reaction complex is correctly reproduced. While such a procedure can be automated, it leads to considerable calculational cost.

An ordering of normal modes with the help of symmetry is generally called adiabatic ordering and has calculational disadvantages, which will be discussed in this work. An appropriate alternative to adiabatic ordering is diabatic ordering, which does not use a symmetry criterion. We will represent here a diabatic ordering method that provides a simple, totally automated way of obtaining the correct curves $\omega_\mu(s)$. This method is not affected by occasionally occurring deviations from the reaction path and, therefore, allows a relatively large step size for reaction valley investigations. Apart from this, it can be set up in a way that the step size is automatically reduced at avoided crossing points and, by this, all avoided crossings are correctly resolved despite the fact that a symmetry criterion is not used in the procedure.

In the next section we discuss the theory of diabatic mode ordering (DMO) and then examine its implementation within an *ab initio* program. The performance of the new method will then be discussed for an application example. Finally, we present general application possibilities of a diabatic ordering of properties depending on some generalized reaction path, which may involve separately or simultaneously geometry changes, mass changes, or force constant changes. The generalized approach can be used to assign vibrational modes of isotopomers or to correlate the vibrational spectra of different molecules.

Theory of Diabatic Ordering of Normal Modes

The geometry of a nonlinear reaction complex with K atoms is fully determined by a set of N = 3K-6 internal coordinates. The direction of the reaction path is given by the gradient $\tilde{\boldsymbol{\gamma}}$ expressed in mass-weighted internal coordinates. In what follows, the tilde indicates mass weighting of a quantity. At a given point of the reaction path, defined by the reaction coordinate s, the generalized normal modes, $\tilde{\mathbf{l}}_\mu^g(s)$, and the associated normal mode frequencies, $\omega_\mu(s)$, are calculated by solving eq. (1):[1, 4, 13–15]

$$\tilde{\mathbf{K}}(s)\tilde{\mathbf{l}}_\mu^g(s) = \omega_\mu^2(s)\tilde{\mathbf{l}}_\mu(s), \qquad \mu = 1, \ldots, N_{vib} \quad (1)$$

which has N_{vib} solutions that span the N_{vib} = 3K-7-dimensional space orthogonal to the one-dimensional reaction path space. Matrix $\tilde{\mathbf{K}}(s)$ is obtained by projection of the force constant matrix $\tilde{\mathbf{F}}(s)$ expressed in mass-weighted internal coordinates from 3K- to 3K-7-dimensional space according to eq. (2):

$$\tilde{\mathbf{K}}(s) = (\mathbf{1} - \tilde{\mathbf{P}}(s))\tilde{\mathbf{F}}(s)(\mathbf{1} - \tilde{\mathbf{P}}(s)) \quad (2)$$

where $\tilde{\mathbf{P}}(s)$ is a projection matrix given by eq. (3):

$$\tilde{\mathbf{P}}(s) = \tilde{\boldsymbol{\gamma}}(s)\tilde{\boldsymbol{\gamma}}^{+}(s) \tag{3}$$

In practice, eq. (1) has to be solved at a discrete set of reaction coordinate values s separated by increments Δs. Assuming that eq. (1) has been solved at two nearby values, s_a and s_b, of the reaction coordinate, eq. (4) follows:

$$\mathbf{K}_a\mathbf{a}_\mu = (\omega_\mu^a)^2\mathbf{a}_\mu \qquad \mu = 1, \ldots, N_{vib} \tag{4a}$$

$$\mathbf{K}_b\mathbf{b}_\mu = \left(\omega_\mu^b\right)^2\mathbf{b}_\mu \qquad \mu = 1, \ldots, N_{vib} \tag{4b}$$

where $\mathbf{a}_\mu$ and $\mathbf{b}_\mu$ denote generalized mass-weighted normal modes calculated at $s = s_a$ and $s = s_b$, respectively, and $\mathbf{K}_a = \tilde{\mathbf{K}}(s_a)$, $\mathbf{K}_b = \tilde{\mathbf{K}}(s_b)$. In eq. (4) and in the following, the tilde, which is used to indicate mass weighting, is dropped for reasons of simplicity. It is useful to collect normal mode vectors $\mathbf{a}_\mu$ and $\mathbf{b}_\mu$ in the $(N \times N_{vib})$ matrices **A** and **B** according to eq. (5):

$$\mathbf{A} = (\mathbf{a}_1, \mathbf{a}_2, \ldots, \mathbf{a}_\mu, \ldots, \mathbf{a}_{N_{vib}}) \tag{5a}$$

$$\mathbf{B} = (\mathbf{b}_1, \mathbf{b}_2, \ldots, \mathbf{b}_\mu, \ldots, \mathbf{b}_{N_{vib}}) \tag{5b}$$

The normal modes of matrices **A** and **B** span the vector spaces $V^{(A)}$ and $V^{(B)}$, respectively. They have to be labeled in such a way that any occasional change in the sequence $1, \ldots, N_{vib}$, because of a crossing of the curves $\omega_\mu(s)$ between points s_a and s_b, is correctly described. Also, degenerate normal modes (at an avoided crossing or at a normal crossing) have to be rotated, so that they can match the old normal modes in the best possible way. Any error in the ordering of normal modes between s_a and s_b will lead to inconsistencies (kinks, etc.) in the representation of $\omega_\mu(s)$, the coupling coefficients $B_{\mu,s}(s)$ and $B_{\mu,\nu}(s)$, or any other on the normal modes' dependent property $X(s)$. In this situation, we apply diabatic mode labeling to avoid any errors in the ordering of normal modes.

Diabatic normal mode labeling as carried out by the DMO method is performed in four steps: (1) at point s_b, the space $V^{(B)}$ is appropriately partitioned into subspaces $V_i^{(B)}$; (2) an image of matrix **A** is calculated in space $V^{(B)}$ and amplitudes $A_\mu^{(i)}$ are calculated to relate each subspace $V_i^{(A)}$ to a subspace $V_i^{(B)}$; (3) the vectors in $V_i^{(B)}$ are rotated to get a correct ordering of normal modes; and (4) a final overlap matrix between **A** and **B** is calculated to check assignments. If necessary, appropriate corrections are made by repeating steps 1–4 for a reduced step size.

The strategy of mode ordering is a backward-directed strategy; that is, for each new point s, the current sequence of frequencies and degree of degeneracy is taken as a fact and the previous ordering of normal mode frequencies is adjusted to the new situation. This is necessary because, at point s_a, it is difficult to predict the degree of degeneracy at point s_b without using symmetry and this will lead to problems as we will show in what follows. However, once modes at s_a have been assigned to those at point s_b, the ordering of the latter is done according to the previous ordering at point s_a.

STEP 1: PARTITIONING OF SUBSPACE $V^{(B)}$

Space $V^{(B)}$, spanned by the vectors $\mathbf{b}_\mu$ $(\mu = 1, \ldots, N_{vib})$, is partitioned according to eq. (6):

$$V^{(B)} = V_1^{(B)} \oplus V_2^{(B)} \oplus \cdots \oplus V_i^{(B)} \oplus \cdots \oplus V_M^{(B)} \tag{6a}$$

$$N_{vib} = N_1 + N_2 + \cdots + N_i + \cdots + N_M \tag{6b}$$

where M is equal to the number of subspaces and N_i indicates the number of vectors $\mathbf{b}_\mu$ with the same frequency $\omega_\mu(s)$ that span the subspace V_i. This is indicated in eq. (7):

$$V_i^{(B)} = \left\{ b_{[\mu i]} \middle| \omega_{[\mu i]}^b = \omega_{[\nu i]}^b; [\mu i], [\nu i] = 1, \ldots, N_i \right\} \tag{7}$$

where the subspace index $[\mu i]$ is used.

STEP 2: RELATING SUBSPACES $V_i^{(A)}$ TO SUBSPACES $V_i^{(B)}$

To each subspace $V_i^{(B)}$, space $V_i^{(A)}$, spanned by vectors $\mathbf{a}_\mu$, has to be related by fulfilling criterion [eq. (8)]:

$$V_i^{(A)} = \{\mathbf{a}_{[\mu i]} | [\mu i] = 1, \ldots, N_i\} \tag{8}$$

The N_i normal modes $\mathbf{a}_{[\mu i]}$ that span subspace $V_i^{(A)}$ are those that possess a large amplitude $A_\mu^{(i)}$ measuring the overlap between $\mathbf{a}_{[\mu i]}$ and subspace $V_i^{(B)}$. If all vectors between two subspaces of **A** and **B** overlap sufficiently, $V_i^{(A)}$ and $V_i^{(B)}$ can be related to each other. Once all vectors have been grouped in related subspaces, the vectors $\mathbf{b}_{[\mu i]}$ in each subspace $V_i^{(B)}$ have to be rotated in such a

way that they match, in the best possible way, vectors $\mathbf{a}_{[\mu i]}$ in subspace $V_i^{(A)}$. This will guarantee that all normal modes smoothly change from point s_a to s_b.

The construction of subspaces $V_i^{(B)}$ (step 1) is straightforward and can easily be automated. However, the construction of spaces $V_i^{(A)}$ is more difficult. To make automatic assignments, one has to quantify how much the vector $\mathbf{a}_\mu$ overlaps with the vectors $\mathbf{b}_\mu$ in space $V_i^{(B)}$. This is a nontrivial problem because of two reasons:

1. The projector $\mathbf{P}(s)$ projects onto the direction of the reaction path, while $1 - P(s)$ projects onto the 3K-7-dimensional space V spanned by the normal modes, which are orthogonal to the reaction path vector. One can consider the 3K-7-dimensional vibrational space as a (hyper)plane, the normal vector of which is the reaction path vector defined by the gradient vector. Any change in the direction of the gradient vector for increasing s leads to a rotation of the vibrational plane (space) V and, as a consequence, also to rotations of the normal modes. Hence, changes in the ordering of the normal modes can be caused by changes in the projector $\mathbf{P}(s)$. In general, $\mathbf{P}(s_a) \neq \mathbf{P}(s_b)$ and, accordingly, space $V^{(B)}$ and space $V^{(A)}$ differ. The global rotation of space $V^{(B)}$ relative to $V^{(A)}$ has to be explicitly taken care of to make an unambiguous identification of normal modes possible. Any type of amplitude, which relates space $V_i^{(B)}$ with vector $\mathbf{a}_\mu$ will be determined by: (a) global rotations of the two spaces relative to each other [i.e., changes of $\mathbf{P}(s)$ along the reaction coordinate]; and (b) individual mixing of normal modes caused by either the diagonalization procedure required to solve eq. (1) (in the case of degenerate modes) or by changes of $\mathbf{F}(s)$. Those two effects have to be separated as will be discussed for step 4.
2. The second difficulty arises from the fact that vectors $\mathbf{a}_\mu$ have to be related to subspaces $V_i^{(B)}$, which implies the definition of a suitable amplitude based on the overlap between vector and subspace.

STEP 2a: CALCULATION OF AN IMAGE OF MATRIX A IN SPACE $V^{(B)}$

Problem 1 can be avoided by simulating vectors $\mathbf{a}_\mu$ with vectors $\mathbf{b}_\mu$. In principle, one can rotate vectors $\mathbf{b}_\mu$ with the help of an unitary matrix $\mathbf{T}$ in such a way that a new set of vectors $\mathbf{a}'_\mu$ is generated, which represents an image of vectors $\mathbf{a}_\mu$ in the space $V^{(B)}$ [see eq. (9)]:

$$\mathbf{A} \approx \mathbf{A}' = \mathbf{BT} \tag{9a}$$

$$Tr(\mathbf{A}^+\mathbf{A}') = \max \tag{9b}$$

$$\mathbf{TT}^+ = \mathbf{I} \tag{9c}$$

It is impossible to find $\mathbf{T}$ such that $\mathbf{A} = \mathbf{A}'$ because the vectors of $\mathbf{A}$ and those of $\mathbf{B}$ span different spaces. Only in the case of $\mathbf{P}(s_a) = \mathbf{P}(s_b)$, which is not true in general, can one find a matrix $\mathbf{T}$ so that $\mathbf{A} = \mathbf{A}'$ holds. The actual value of $Tr(\mathbf{A}^+\mathbf{A}')$ in eq. (9b) can indicate whether it is possible to assign the normal modes associated with matrix $\mathbf{A}$ correctly. In addition, eq. (9) will automatically take care of possible permutations of modes $\mathbf{a}_\mu$ relative to $\mathbf{b}_\mu$.

The matrix $\mathbf{T}$, which fulfills eq. (9b), is given by eq. (10):

$$\mathbf{T} = (\mathbf{S}_{AB}^+\mathbf{S}_{AB})^{-1/2}\mathbf{S}_{AB}^+ \tag{10}$$

where:

$$\mathbf{S}_{AB} = \mathbf{A}^+\mathbf{B} \tag{11}$$

is the matrix that describes the overlap between vectors $\mathbf{a}_\mu$ and $\mathbf{b}_\mu$.

STEP 2b: DEFINITION OF AN APPROPRIATE AMPLITUDE

The procedure given in eq. (9) takes care of global rotations of spaces $V^{(B)}$ and $V^{(A)}$ relative to each other, leading to possible permutations of normal modes. To solve the problem of assigning N_i vectors in space $V^{(A)}$ to N_i vectors in space $V_i^{(B)}$, an appropriate amplitude will be defined.

Utilizing the inverse of matrix $\mathbf{T}$ defined in eq. (9), vectors $\mathbf{b}_\mu$ can be expressed in terms of vectors $\mathbf{a}'_\mu$ according to eq. (12):

$$\mathbf{b}_\mu = \sum_{\nu=1}^{N_{vib}} \mathbf{a}'_\nu T_{\nu\mu}^+ \tag{12}$$

It is convenient to construct the projector, $\mathbf{P}_i^{(B)}$, onto the space $V_i^{(B)}$:

$$\mathbf{P}_i^{(B)} = \sum_{[\mu i]=1}^{N_i} \mathbf{b}_{[\mu i]}\mathbf{b}_{[\mu i]}^+ \tag{13}$$

By using eq. (12), one obtains eq. (14):

$$\mathbf{P}_i^{(B)} = \sum_{\lambda,\,\sigma=1}^{N_{vib}} \mathbf{a}'_\lambda \mathbf{a}'^{+}_\sigma \sum_{[\mu i]=1}^{N_i} T_{[\mu i],\lambda} T_{[\mu i],\sigma} \quad (14)$$

Because eq. (15) holds:

$$N_i = Tr(\mathbf{P}_i^{(B)}) \quad (15)$$

it is possible to obtain eq. (16):

$$1 = \sum_{\lambda=1}^{N_{vib}} A_\lambda^{(i)} \quad (16)$$

where:

$$A_\lambda^{(i)} = \frac{1}{N_i} \sum_{[\mu i]=1}^{N_i} T^2_{[\mu i],\lambda} \quad (17)$$

The N_i normal modes $\mathbf{a}_\mu$ with largest amplitude values $A_\lambda^{(i)}$ can be assigned to space $V_i^{(A)}$.

The transformation of eqs. (13) into (14) is essential for determining amplitudes $A_\mu^{(i)}$ because it is the basis for relating the space $V_i^{(B)}$ [described by the projector $\mathbf{P}_i^{(B)}$] with vectors $\mathbf{a}_\mu$ of space $V^{(A)}$. In addition, the procedure of finding image vectors $\mathbf{a}'_\mu$, which mimic vectors $\mathbf{a}_\mu$ in space $V^{(B)}$ [see eq. (9)] is the only way of connecting the vectors of spaces $V^{(B)}$ and $V^{(A)}$ because, in general, it is not possible to express vectors $\mathbf{b}_\mu$ in terms of $\mathbf{a}_\mu$. Because the two spaces are rotated with regard to each other, the image vectors $\mathbf{a}'_\mu$ cannot be replaced by vectors $\mathbf{a}_\mu$, and the use of image vectors in eq. (12) cannot be avoided when constructing amplitudes $A_\mu^{(i)}$.

STEP 3: ROTATION OF VECTORS $\mathbf{B}_\mu$ IN SUBSPACE $V_i^{(B)}$

Finally, vectors $\mathbf{b}_\mu$ in subspace $V_i^{(B)}$ are rotated according to eq. (18):

$$\mathbf{b}'_{[\mu i]} = \sum_{[\nu i]=1}^{N_i} \mathbf{b}_{[\nu i]} R^i_{[\nu i],[\mu i]}, \qquad [\mu i] = 1, \ldots, N_i \quad (18)$$

where $\mathbf{R}_i$ is the rotation matrix associated with space $V_i^{(B)}$:

$$\mathbf{R}^i = \left[(\mathbf{S}^i_{AB})^+ \mathbf{S}^i_{AB} \right]^{-1/2} (\mathbf{S}^i_{AB})^+ \quad (19)$$

and $\mathbf{S}^i_{AB}$ is the overlap matrix for space $V_i^{(B)}$ given by eq. (20):

$$(\mathbf{S}^i_{AB})_{[\mu i],[\nu i]} = \mathbf{a}^+_{[\mu i]} \mathbf{b}_{[\nu i]}, \quad [\mu i], [\nu i] = 1, \ldots, N_i \quad (20)$$

This leads to the correct ordering of degenerate modes spanning subspace $V_i^{(B)}$. It is convenient to arrange ordered and rotated vectors $\mathbf{b}_{[\mu i]}$ ($i = 1, \ldots, M$; $[\mu i] = 1, \ldots, N_i$) in matrix $\mathbf{B}'$ columnwise.

STEP 4: TESTING OF FINAL ASSIGNMENTS

Once all normal modes are ordered and degenerate modes are rotated, it is simple to test assignments by calculating the final overlap matrix $\mathbf{S}_{AB}$ according to eq. (21), which should be close to diagonal.

$$(\mathbf{S}_{AB})_{\mu\nu} = \mathbf{a}^+_\mu \mathbf{b}'^{+}_\mu \quad (21)$$

In addition, one can define a single characteristic amplitude of assignment defined by the smallest value of $\mathbf{S}_{AB}$:

$$A(\mathbf{A}, \mathbf{B}') = \min\left\{ (S_{AB})_{\mu,\mu} \middle| \mu = 1, \ldots, N_{vib} \right\} \quad (22)$$

If A is smaller than a threshold $S_{\min}$, the assignment will be considered weak and, therefore, it must be repeated, as will be described in the next section.

The assignment amplitude defined in eq. (22) accounts for the rotation of the projection plane [i.e., the change of $\mathbf{P}(s)$ along the reaction path] and normal mode mixing resulting from a change of $\mathbf{F}(s)$. These two effects have to be separated to gain better control over the assignment of normal mode vectors $\mathbf{a}_\mu$. It is possible to define an amplitude $A(\mathbf{A}, \mathbf{A}')$, which only measures the degree of rotation caused by the change of $\mathbf{P}(s)$ when going from s_a to s_b:

$$A(\mathbf{A}, \mathbf{A}') = \min\{ (\mathbf{A}^+ \mathbf{A}')_{\mu\mu} \big| \mu = 1, \ldots, N_{Vib} \} \quad (23)$$

where $\mathbf{A}'$ is given by eq. (9).

The simultaneous usage of $A(\mathbf{A}, \mathbf{B}')$ and $A(\mathbf{A}, \mathbf{A}')$ is important when there are large changes in the projector $\mathbf{P}(s)$ along the reaction path and, accordingly, space $V^{(B)}$ is considerably rotated relative to space $V^{(A)}$. This can happen if a too-large step size Δs is used for the investigation of a particular reaction path. In such a case, it is difficult to assign the normal modes at point s_a to those at point s_b because all amplitudes $A_\mu^{(i)}$ will

have relatively small values. This situation can be controlled with the help of amplitude $A(\mathbf{A}, \mathbf{A}')$: The step size is reduced as long as amplitude $A(\mathbf{A}, \mathbf{A}')$ is smaller than the threshold value $S_{\min}$. For that step size which leads to a sufficiently large amplitude $A(\mathbf{A}, \mathbf{A}')$ additional problems in assigning normal modes caused by changes in $\mathbf{F}(s)$ can exist. For example, at an avoided crossing, $\mathbf{F}(s)$ changes considerably and, accordingly, amplitude $A(\mathbf{A}, \mathbf{B}')$ could be smaller than $S_{\min}$. Further reduction of the step size controlled by the value of amplitude $A(\mathbf{A}, \mathbf{B}')$, which in this situation includes only effects of $\mathbf{F}(s)$, would lead to a resolution of the avoided crossing. Hence, requiring that both $A(\mathbf{A}, \mathbf{A}')$ and $A(\mathbf{A}, \mathbf{B}')$ are larger than $S_{\min}$ guarantees a correct correlation of normal modes at two neighboring points along the reaction path and represents the final check of the DMO method.

Implementation of DMO Method

The possibility of quantifying the assignment of vectors $\mathbf{a}_\mu$ to vectors $\mathbf{b}_\mu$ is the basis for the implementation of self-correcting algorithms. There are two basic strategies of generating generalized normal modes $\omega(s)$: the first uses a fixed and the second a variable step size along the reaction path, which will be discussed next.

USE OF A FIXED STEP SIZE

The use of a fixed step size, $\Delta s = s_n - s_{n-1} =$ const, where the constant (typically ≤ 0.01 amu$^{1/2}$ Bohr) is chosen to be so small that assignment amplitudes are mostly larger than a threshold value $S_{\min} = 0.999$. This procedure will be suitable if the calculation of points along the reaction path is not costly. The procedure comprises the following steps:

1. The reaction path is generated by calculating the energy, energy gradient, and force constant matrix at a certain sequence of points $s_1, s_2, \ldots, s_n, \ldots, s_p$, where the spacing between the points is given by Δs.
2. Labeling of normal modes is carried out for point s_1 according to increasing (decreasing) values of the corresponding normal mode frequencies. The normal mode vectors are stored in matrix $\mathbf{A}$ [eq. (5a)].
3. The normal modes calculated at point s_n (if step 3 is entered from step 2 rather than step 4, then $s_n = s_2$) are stored in matrix $\mathbf{B}$ [eq. (5b)] and ordered according to eqs. (6)–(20) so that they match modes $\mathbf{a}_\mu$ collected in matrix $\mathbf{A}$.
4. The characteristic assignment amplitudes $A(\mathbf{A}, \mathbf{B}')$ and $A(\mathbf{A}, \mathbf{A}')$ defined in eqs. (22) and (23) are calculated. If both amplitudes are larger than $S_{\min} = 0.999$, then all assignments can be accepted, matrix $\mathbf{B}$ is stored in $\mathbf{A}$, and the procedure continues with step 3 provided the final point s_p has not been reached. If amplitudes $A(\mathbf{A}, \mathbf{B}')$ and $A(\mathbf{A}, \mathbf{A}')$ are smaller than $S_{\min}$, improved assignments will have to be made according to step 5.
5. The amount of rotation of space $V^{(B)}$ with regard to $V^{(A)}$ can be reduced if the increment Δs is decreased and a new point s_n^* is included in the sequence of points used to describe the reaction path. In principle, one could calculate $\mathbf{P}(s_n^*)$, $\mathbf{F}(s_n^*)$, $\mathbf{K}(s_n^*)$, and $\mathbf{I}_\mu(s_n^*)$ [eqs. (1)–(3)] and repeat steps 2, 3, and 4 for s_n^* to obtain improved assignments. However, this would lead to a awkward calculational procedure and extensive restoring of properties calculated along the reaction path. If the increment Δs is chosen to be rather small from the beginning one can refrain from explicitly calculating $\mathbf{P}(s_n^*)$, $\mathbf{F}(s_n^*)$, $\mathbf{K}(s_n^*)$, and $\mathbf{I}_\mu(s_n^*)$ and, instead, use the linear interpolation formula eq. (24):

$$\mathbf{P}(s_n^*) = \mathbf{P}(s_n)\frac{s_n^* - s_{n-1}}{s_n - s_{n-1}} + \mathbf{P}(s_{n-1})\frac{s_n^* - s_n}{s_{n-1} - s_n} \tag{24a}$$

$$\mathbf{F}(s_n^*) = \mathbf{F}(s_n)\frac{s_n^* - s_{n-1}}{s_n - s_{n-1}} + \mathbf{F}(s_{n-1})\frac{s_n^* - s_n}{s_{n-1} - s_n} \tag{24b}$$

to obtain $\mathbf{P}(s_n^*)$ and $\mathbf{F}(s_n^*)$ for an improved assignment. Repeated application of eq. (22) may be necessary to get a characteristic assignment amplitude ≥ 0.999.

USE OF A VARIABLE STEP SIZE

The use of a variable step size leads to a decrease of computational cost because the larger the increment Δs the smaller the number of points s_n to be calculated. A procedure based on a variable step size differs from the one with fixed step size insofar as fixing of Δs and mode ordering is done as soon as energy, energy gradient, and force con-

stant matrix are calculated for a new point s_n. The procedure covers the following computational steps:

1. After calculating and storing normal mode vectors $\mathbf{a}_\mu$ in matrix **A**, a relatively large trial step size $\Delta s_{\max}$ is chosen, which depends on the reaction system investigated.
2. After calculating **P**, **F**, and the normal modes at $s_{n+1} = s_n + \Delta s_{\max}$, storage of $\mathbf{b}_\mu$ in **B**, ordering according to eqs. (6)–(20), and calculation of the characteristic amplitudes $A(\mathbf{A}, \mathbf{B}')$ and $A(\mathbf{A}, \mathbf{A}')$ is carried out. If these are both larger than $S_{\min} = 0.999$, then steps 1 and 2 will be done for the next point, otherwise step 3 has to be performed.
3. To increase the overlap between **A** and **B**, Δs is scaled by a reduction factor $\lambda > 0$ to obtain a new point s_n^* between s_n and s_{n+1}:

$$s_n^* = \lambda s_n + (1 - \lambda) s_{n+1} \qquad (25)$$

where λ is determined according to the calculated values of the characteristic amplitudes. The normal modes calculated at point s_n^* lead to larger amplitudes $A(\mathbf{A}, \mathbf{B}')$ and $A(\mathbf{A}, \mathbf{A}')$ than those calculated at s_{n+1}. This procedure can be repeated until $A(\mathbf{A}, \mathbf{B}')$ and $A(\mathbf{A}, \mathbf{A}')$ become larger than $S_{\min}$.

Clearly, step 3 will only be necessary at points where electronic changes occur, otherwise large step sizes can be used. In this way, smooth functions, $\omega(s)$, are obtained with relatively low computational cost, which is an advantage when the calculation of energy, energy gradient, and force constant matrix at each point along the reaction path is expensive.

In its present version DMOL uses a fixed step size, while a fully automated version with variable step size is under development. DMOL is a part of the ADIA program[16] that carries out unified reaction valley analysis (URVA)[17] within the *ab initio* package COLOGNE96.[18] Next, we present a test example to demonstrate the usefulness of the DMO method.

APPLICATION OF DMO

Diabatic mode ordering was tested for reaction (26):[18–20]

$$CH_3 + H_2 \rightarrow CH_4 + H \qquad (26)$$

which has been studied with the help of the RPH by various investigators at different levels of theory.[21–28,5,11] Because the primary goal of this work is to test the usefulness of DMOL rather than to investigate the reaction mechanism of reaction (26), its reaction path was generated at the UHF/STO-3G level of theory, applying the method suggested by Gonzales and Schlegel.[29]

Figure 1 shows calculated generalized normal mode frequencies $\omega(s)$ in the range from -3 to 3 amu$^{1/2}$ Bohr of the reaction path using a fixed step size of 0.05 amu$^{1/2}$ Bohr. Because this step size is relatively large, the DMO method cannot resolve an avoided crossing involving $\omega(s)$ of modes $2a_1$ (mode 8) and $3a_1$ (mode 11), which occurs between $s = -0.3$ and -0.25 amu$^{1/2}$ Bohr. Modes $2a_1$ and $3a_1$ interact so weakly in this region that they approach each other rather closely. Even if the avoided crossing is resolved by DMO, one has to enlarge the representation in Figure 1 to see that the curves $\omega(s)$ indeed do not cross.

The consequences of missing the avoided crossing between $s = -0.3$ and -0.25 amu$^{1/2}$ Bohr are shown in Figure 2, where the reaction path curvature $\kappa(s)$ and the normal mode-curvature coupling coefficients $B_{\mu,s}$ are given as a function of s. At the position of the avoided crossing, the function $B_{2a1,s}(s)$ possesses a kink that is a direct consequence of an erroneous mode ordering after the nonresolved avoided crossing shown in Figure 1.

The avoided crossing between $s = -0.3$ and -0.25 amu$^{1/2}$ Bohr can be resolved by reducing the step size as described previously. In Figures 3 and 4, results are shown for the region $-3 \le s \le 3$ amu$^{1/2}$ Bohr (compare with Fig. 1) where the insert in Figure 3 provides a better view of $\omega(s)$ in the region of the avoided crossing. In Figure 5, individual amplitudes $A(\mathbf{A}, \mathbf{B}')_{\mu\mu} = (\mathbf{A}^+\mathbf{B}')_{\mu\mu}$ for a_1- and e-symmetrical vibrational modes are shown as a function of reaction coordinate s for the situation of the unresolved avoided crossing, whereas in Figure 6, characteristic amplitudes $A(\mathbf{A}, \mathbf{B}')$ and $A(\mathbf{A}, \mathbf{A}')$ are given before (Fig. 6a) and after resolving the avoided crossing between $s = -0.3$ and -0.25 amu$^{1/2}$ Bohr (Fig. 6b).

The amplitudes $A(\mathbf{A}^+\mathbf{B}')_{\mu\mu}$ of modes $2a_1$ and $3a_1$ become relatively small (relative to $S_{\min} = 0.999$) at $s = -0.26$ ($A_{2a1} = 0.954$; $A_{3a1} = 0.938$), of modes $1a_1$ and $3a_1$ at $s = 0.24$ ($A_{1a1} = 0.976$; $A_{3a1} = 0.977$) and of modes $2a_1$ and $3a_1$ at $s = 0.57$ amu$^{1/2}$ Bohr ($A_{2a1} = 0.971$; $A_{3a1} = 0.965$) (Fig. 5) thus indicating that these mode pairs are involved in avoided crossings at the locations given. Simi-

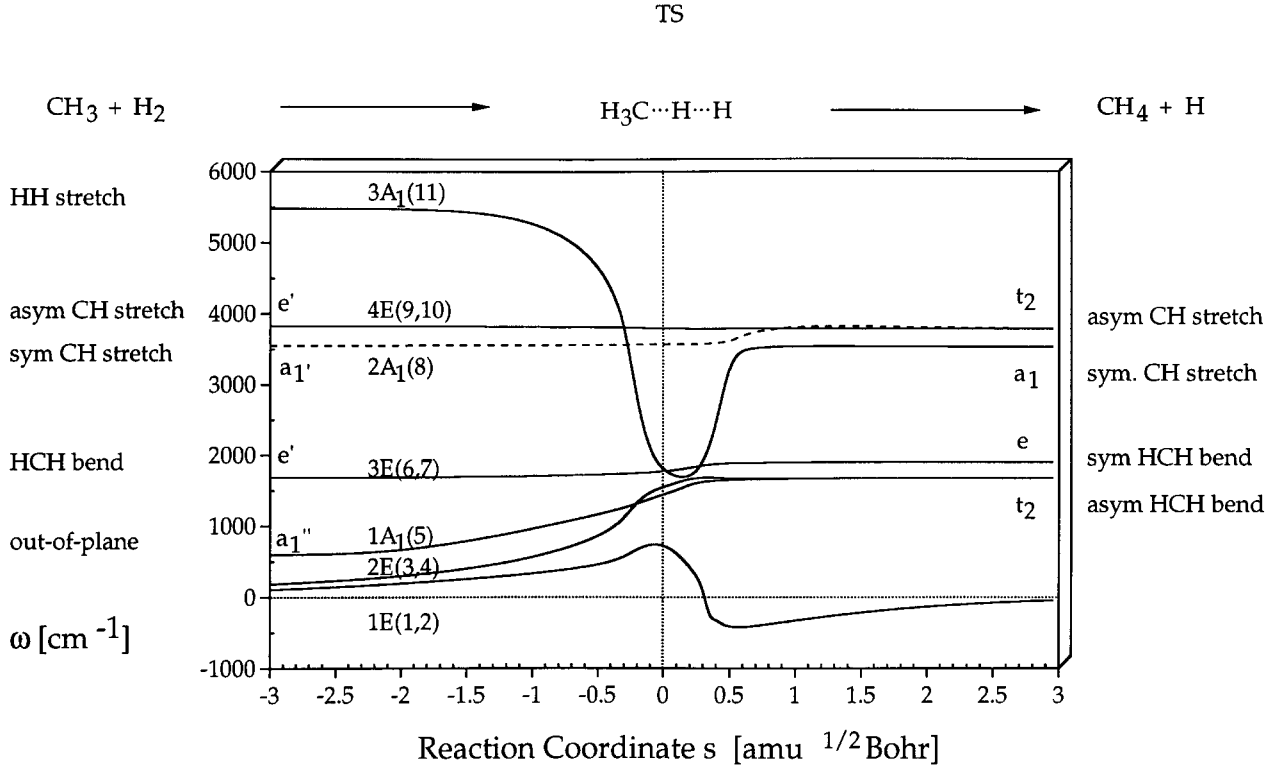

FIGURE 1. Diabatic representation of normal mode frequencies $\omega_\mu(s)$ calculated at the UHF / STO-3G level of theory for the reaction $CH_3 + H_2 \rightarrow CH_4 + H$ using a fixed step size, $\Delta s = 0.05$ amu$^{1/2}$ Bohr. Symmetry symbols (CH_3: D_{3h}; CH_4: T_d symmetry) and characterization of normal modes are indicated both with regard to reactants and products. The numbering of the normal modes of the C_{3v}-symmetrical reaction complex is done in the entrance channel ($s < 0$) from small to large frequencies. The function $\omega(s)$ of the $2a_1(8)$ vibrational mode is dashed to show that the avoided crossing with the $3a_1(11)$ mode is not resolved at the step size chosen. The position of the transition state corresponds to $s = 0$ amu$^{1/2}$ Bohr.

larly, the corresponding amplitudes for the *e*-symmetrical modes $2e$ and $3e$ indicate avoided crossings at $s = -0.06$ and $s = 0.19$ amu$^{1/2}$ Bohr. Because the avoided crossing involving modes $2a_1$ and $3a_1$ at $s = -0.26$ amu$^{1/2}$ Bohr is not resolved (Fig. 1), the labeling of these two modes for any $s > -0.26$ amu$^{1/2}$ Bohr must be erroneous.

The characteristic amplitudes $A(\mathbf{A}, \mathbf{B}')$ and $A(\mathbf{A}, \mathbf{A}')$, shown in Figure 6a and b, summarize the results of Figure 5. It is noteworthy that amplitude $A(\mathbf{A}, \mathbf{B}')$, which covers the effects of both $\mathbf{P}(s)$ and $\mathbf{F}(s)$, is considerably smaller than amplitude $A(\mathbf{A}, \mathbf{A}')$ at the nonresolved avoided crossing point. As discussed in the previous section, amplitude $A(\mathbf{A}, \mathbf{A}')$ provides a measure for rotation of the projection plane at the avoided crossing point, which is related to the curvature of the reaction path. As can be seen from Figure 2, this is larger at $s = 0.5$ than at $s = -0.3$ amu$^{1/2}$ Bohr, which is confirmed by the corresponding values of $A(\mathbf{A}, \mathbf{A}')$ (see Fig. 6a). If, beside rotation of the projection plane, the changes in $\mathbf{F}(s)$ are also covered by the characteristic amplitude, as is the case for $A(\mathbf{A}, \mathbf{B}')$, a smaller value of A will result.

As can be seen from Figure 3, the application of a reduced step size in the range between $s = -0.3$ and -0.25 amu$^{1/2}$ Bohr prevents that the curves $\omega(s)$ of normal modes $2a_1$ and $3a_1$ cross, even though the two curves approach each other closely. The correct ordering of normal modes $2a_1$ and $3a_1$ at the avoided crossing point leads to drastic changes in the decomposition of the reaction path curvature in normal mode components, as shown in Figure 4. After resolving the avoided crossing, it becomes obvious that the two curvature components $B_{2a1,s}$ and $B_{3a1,s}$ contribute almost equally to the curvature peak at $s = -0.3$ amu$^{1/2}$ Bohr. For $s < -0.28$ amu$^{1/2}$ Bohr the $3a_1$ component dominates, and for $s > -0.28$ amu$^{1/2}$ Bohr the $2a_1$ component dominates, while component $3a_1$ seems to be dominating in the whole range when the avoided crossing between $s = -0.3$ and -0.25

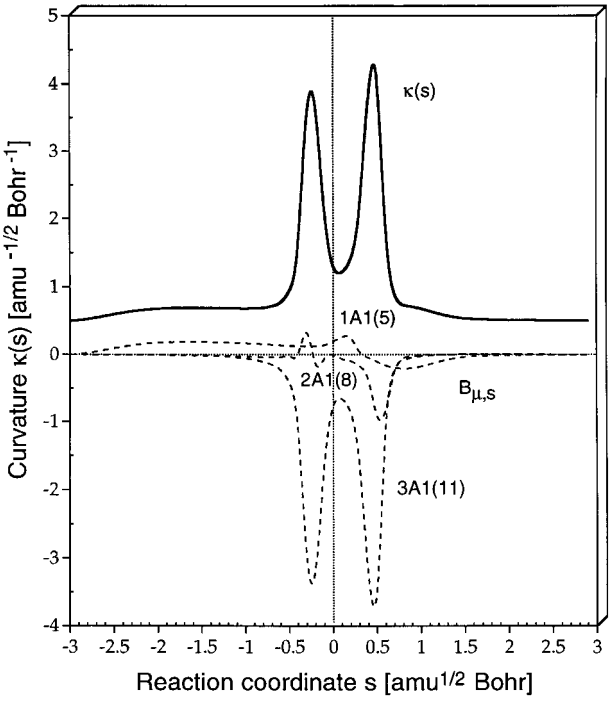

FIGURE 2. Characterization of the reaction path curvature $\kappa(s)$ (thick solid line) in terms of curvature coupling coefficients $B_{\mu,s}(s)$ (dashed lines). The function $\kappa(s)$ has been shifted by 0.5 amu$^{-1/2}$ Bohr^{-1} to better distinguish between reaction path curvature $\kappa(s)$ and curvature coupling coefficients $B_{\mu,s}(s)$. Symmetry symbols and numbering of normal modes (in parentheses) are indicated. The position of the transition state corresponds to $s = 0$ amu$^{1/2}$ Bohr.

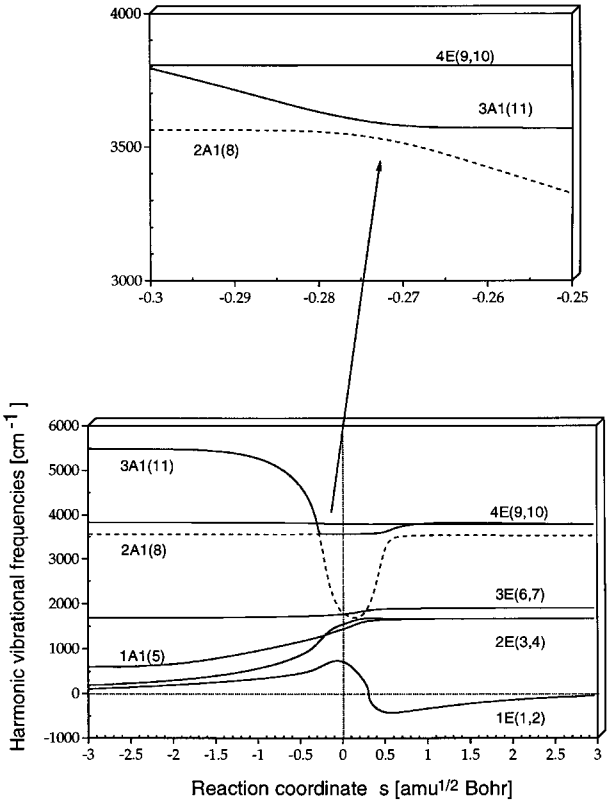

FIGURE 3. Diabatic representation of normal mode frequencies $\omega_\mu(s)$ in the region $-3 \le s \le 3$ amu$^{1/2}$ Bohr using a reduced step size. The function $\omega(s)$ of the $2a_1(8)$ vibrational mode is dashed to show that the avoided crossing with the $3a_1(11)$ mode is resolved. This is shown more clearly by enlarging the region $-0.3 \le s \le -0.25$ amu$^{1/2}$ Bohr as is done in the upper half of the figure.

amu$^{1/2}$ Bohr is not resolved (Fig. 2). For the second curvature peak, the $2a_1$ component is much larger (Fig. 4) than the $3a_1$ component (Fig. 2). Hence, the unresolved avoided crossing shown in Figure 1 leads not only to the kink in the $2a_1$ component (Fig. 2) but also to the wrong decomposition of the two curvature peaks between $s = -0.3$ and $s = 0.5$ amu$^{1/2}$ Bohr (Fig. 2).

The two curvature peaks are related to changes in the direction of the reaction path when described as a function of the HH distance $R1$ and the CH distance $R2$ (see Fig. 7). The first curvature peak at $s = -0.3$ amu$^{1/2}$ Bohr (Fig. 4) corresponds to curvature $k1$ in the $R1/R2$ diagram and the second curvature peak at 0.5 amu$^{1/2}$ Bohr to curvature $k2$; that is, the curvature peaks of the $CH_3 + H_2$ reaction path are dominated by changes in the HH distance $R1$ (first curvature peak) and the CH distance (second curvature peak).

At a step size of 0.01 amu$^{1/2}$ Bohr, the avoided crossing is resolved which is indicated by an amplitude $A(\mathbf{A}, \mathbf{A}') > 0.999$ for all s values considered. However, amplitude $A(\mathbf{A}, \mathbf{B}')$ at the avoided crossing point, which describes changes in matrix $\mathbf{F}(s)$, drops from 0.94 to 0.75, contrary to what one might expect in view of the smaller step size. We note that the reduction of amplitude $A(\mathbf{A}, \mathbf{B}')$ is, first of all, a numerical effect that results from the fact that the avoided crossing point is better located with a step size of 0.01 rather than 0.05 amu$^{1/2}$ Bohr and, accordingly, numerically better described. The same is true for the peaks of curvature $\kappa(s)$, for which reliable values can only be obtained using a sufficiently small step size.

In the present case, investigation of amplitude $A(\mathbf{A}, \mathbf{A}')$ is sufficient to correctly describe the avoided crossing at $s = -0.28$ amu$^{1/2}$ Bohr and the additional reduction of the step size to fulfill the criterion $A(\mathbf{A}, \mathbf{B}') > S_{\min} = 0.999$ is not necessary. However, for the general case, both $A(\mathbf{A}, \mathbf{A}')$

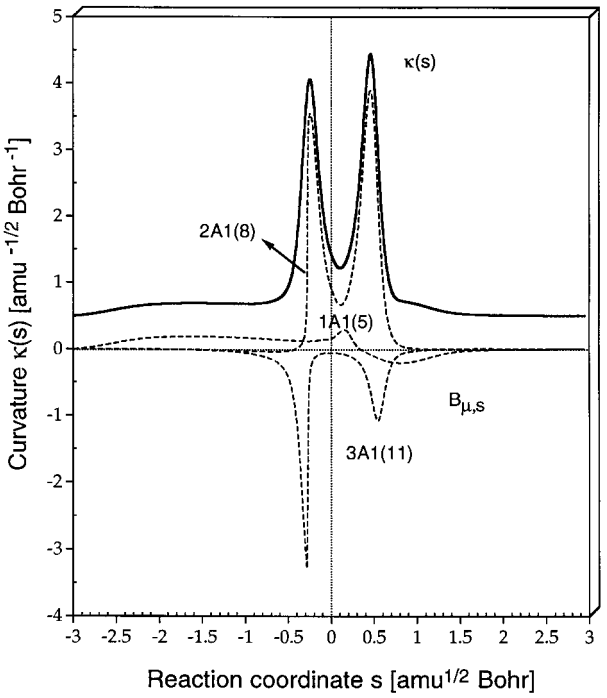

FIGURE 4. Characterization of the reaction path curvature $\kappa(s)$ (thick solid line) in terms of curvature coupling coefficients $B_{\mu,s}(s)$ (dashed lines) after correction of normal mode ordering with the help of a reduced step size Δs. The function $\kappa(s)$ has been shifted by 0.5 amu$^{-1/2}$ Bohr^{-1} to better distinguish between reaction path curvature $\kappa(s)$ and curvature coupling coefficients $B_{\mu,s}(s)$.

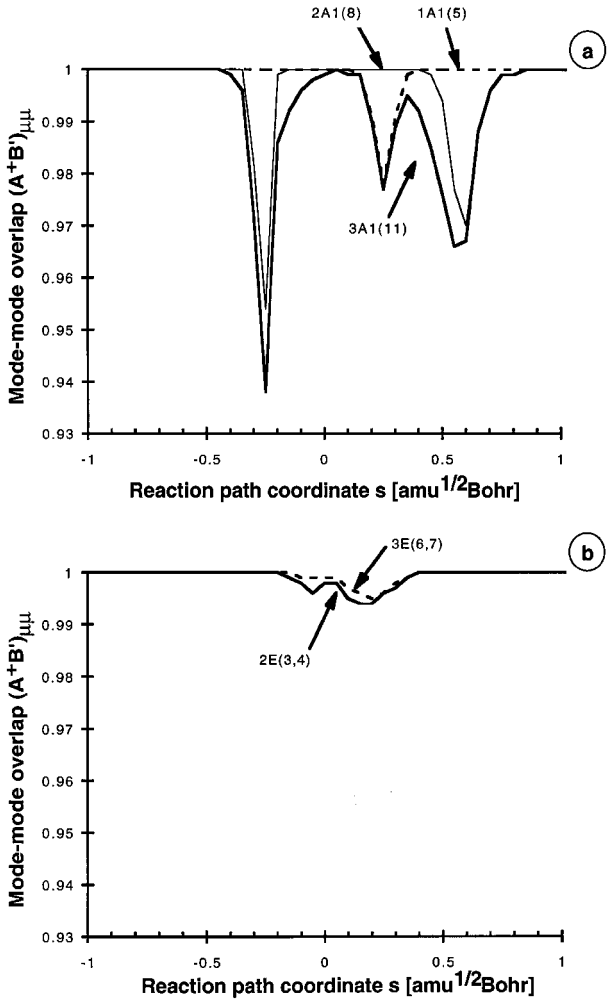

FIGURE 5. Amplitudes $A(\mathbf{A}, \mathbf{B}')_{\mu\mu}$ calculated for (a) a_1-symmetrical and (b) e-symmetrical normal modes of the reaction complex $CH_3 \cdots H_2$ as a function of the reaction coordinate. Numbers in parentheses correspond to the numbering of normal modes given in Figure 1 and 3 (UHF / STO-3G calculations).

and $A(\mathbf{A}, \mathbf{B}')$ have to be investigated to make sure that all avoided crossings are described correctly. Future work has to clarify when these rather stringent conditions can be relaxed.

General Application Possibilities

Diabatic ordering described in this work can also be applied to other properties that depend on a reaction coordinate s. Some examples are given next.

In reaction path studies it may be of interest that the orbital energies, ε, of the reaction complex are investigated as a function of s, $\varepsilon(s)$. The problem of labeling molecular orbitals (MO) resembles that of labeling normal modes. Partitioning of the total space at point s_n depends on the degree of degeneracy of MOs. If the MOs are represented by the vector $\mathbf{c}_\mu$, the elements of which are the coefficients of a LCAO expansion, then the overlap between the MOs at subsequent points s_n and s_{n+1} will be determined in the same way as the overlap between normal modes at these points. Similar considerations will apply if one wants to study changes in the energy of ground and excited states, $E_i(s)$, along the reaction path.

Another problem that can be solved by the diabatic labeling procedure just described is the correct assignment of normal modes that belong to different isotopomers. This becomes obvious when one uses the change in mass from one isotopomer to the other as a reaction coordinate. Then, a stepwise change in mass will convert one isotopomer into the other comparable to a rearrangement reaction between two isomers. Hence, isotopomer fre-

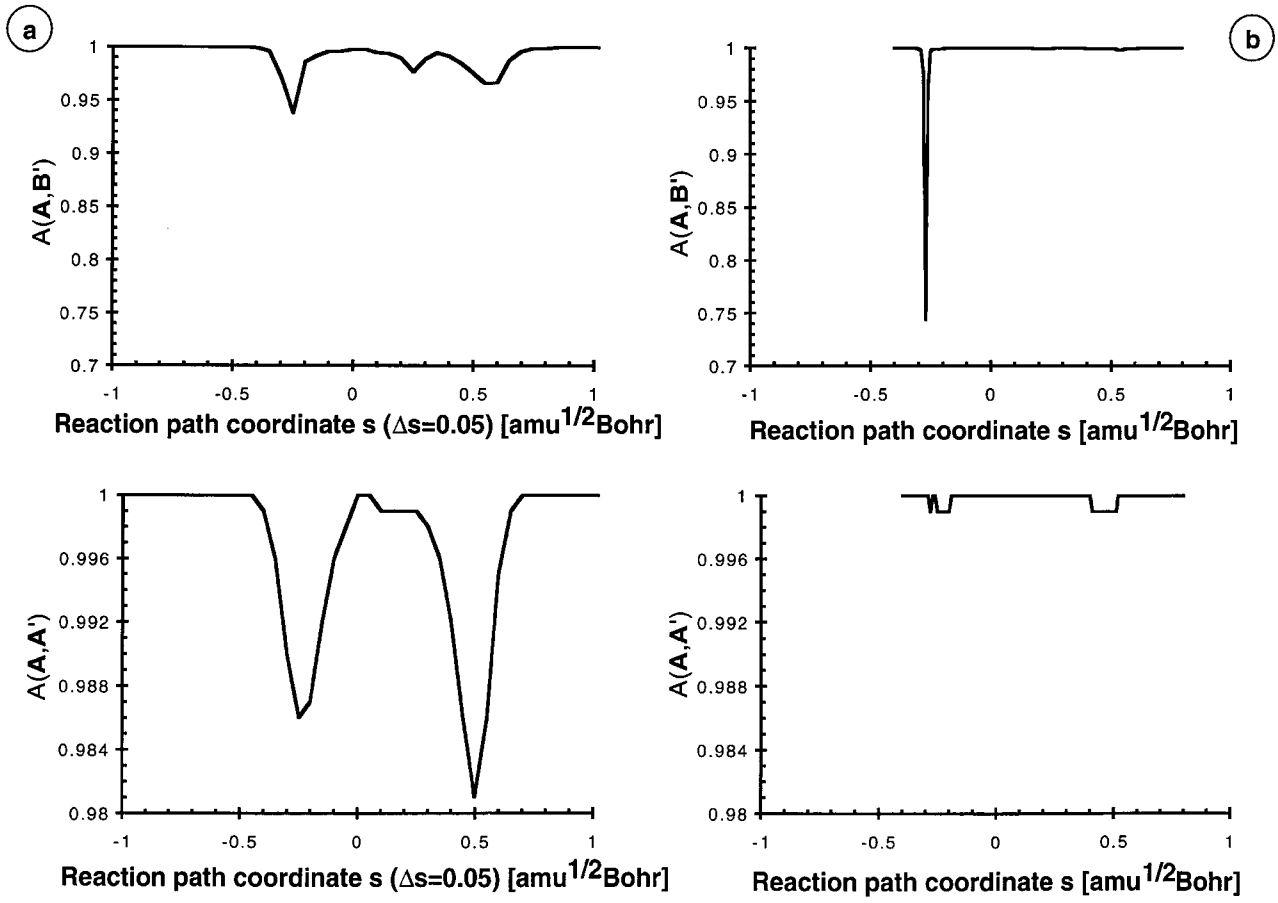

FIGURE 6. Amplitudes $A(\mathbf{A}, \mathbf{B}')$ and $A(\mathbf{A}, \mathbf{A}')$ dependent on the reaction coordinate s calculated (a) before resolution of the avoided crossing at $s = -0.28$ amu$^{1/2}$ Bohr (step size $\Delta s = 0.05$ amu$^{1/2}$ Bohr) and (b) after resolution of the avoided crossing by locally reducing the step size to 0.01 amu$^{1/2}$ Bohr.

quencies can be related to each other using a mass-dependent reaction coordinate s and the DMO method.

In a particular case, two isotopomers $l1$ and $l2$ may differ with regard to the masses of L of their atoms. The masses which differ can be aligned in two column vectors $\mathbf{u}_1$ and $\mathbf{u}_2$:

$$\mathbf{u}_1 = (m_1^{(1)}, m_2^{(1)}, \ldots, m_L^{(1)})^+ \quad (27a)$$

$$\mathbf{u}_2 = (m_1^{(2)}, m_2^{(2)}, \ldots, m_L^{(2)})^+ \quad (27b)$$

The generalized reaction path connecting the two isotopomers is given by the vector function $\mathbf{u}(s)$ with components defined in eq. (28):

$$\mathbf{u}(s) = (m_1(s), m_2(s), \ldots, m_L(s))^+ \quad \text{for } 0 < s < 1 \quad (28)$$

and the boundary conditions:

$$\mathbf{u}(0) = \mathbf{u}_1, \mathbf{u}(1) = \mathbf{u}_2 \quad (29)$$

Because there is no criterion that determines $\mathbf{u}(s)$, an infinite number of paths connecting $\mathbf{u}_1$ and $\mathbf{u}_2$ exists and the parameterization of $\mathbf{u}(s)$ is arbitrary. A simple parameterization is given by:

$$\mathbf{u}(s) = (1 - s)\mathbf{u}_1 + s\mathbf{u}_2 \quad (30)$$

Once $\mathbf{u}(s)$ is chosen, diabatic labeling of normal modes is straightforward because the vibrational equation [eq. (31)] can be parameterized with the help of s:

$$\mathbf{F}\mathbf{d}_\mu(s) = \omega_\mu^2(s)\mathbf{G}^{-1}(s)\mathbf{d}_\mu(s) \quad (31)$$

In this case, the force constant matrix $\mathbf{F}$ is independent of s and, therefore, it has to be calculated just

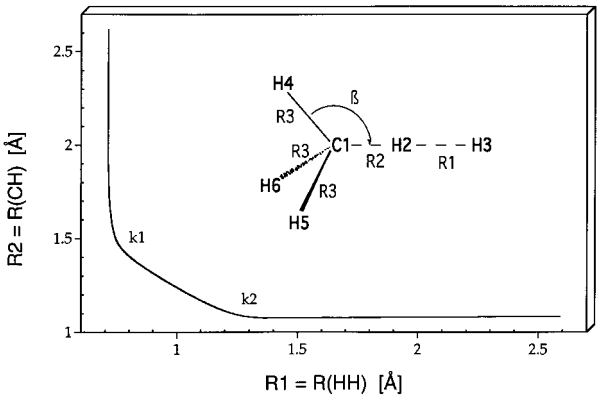

FIGURE 7. The reaction path of the reaction $CH_3 + H_2 \rightarrow CH_4 + H$ given as a function of the HH distance $R1$ and the CH distance $R2$. The path curvatures $k1$ and $k2$ correspond to the curvature peaks of Figure 4.

for $s = 0$. Because of this, the calculational cost for diabatic mode ordering in the case of isotopomers is small.

Another problem of interest, which can be solved with DMO, is the question of whether the vibrational spectra of two closely related molecules such as benzene and toluene can be correlated using the procedure described for isotopomers. Prerequisite for such a procedure is the definition of a generalized reaction path vector **u** which covers changes in geometry (described by internal coordinates q_n), masses, and force constant matrix elements:

$$\mathbf{u}(s) = (q_n; n = 1, \ldots, N \,|\, m_1, m_2, \ldots m_K \,|\, F_{nm}; \; n, m = 1, \ldots, N)^+ \tag{32}$$

The force constant matrix **F** has to be calculated at $s = 0$ and $s = 1$ and, for intermediate points, a formula similar to eq. (24b) has to be applied. Using step sizes $\Delta s = \Delta s(\Delta q_n, \Delta m, \Delta \mathbf{F})$ for a sequence of points between $s = 0$ and $s = 1$ normal modes are calculated and ordered with DMO so that an exact correlation of vibrational spectra is possible. Work is in progress to clarify the extent to which such a method can be applied to vibrational spectra of molecules with increasingly different structures.

Conclusions

In this work, we have presented a new method of diabatic mode ordering (DMO) that can be applied in connection with reaction path investigations. The advantages of the DMO method are:

1. DMO does not use symmetry and, accordingly, can be applied in situations where the symmetry of the reaction complex changes along the reaction path, as for example, at a bifurcation point.
2. The assignment of normal modes at different points s_n and s_{n+1} can be quantified by calculating the characteristic assignment amplitudes $A(\mathbf{A}, \mathbf{B}')$ and $A(\mathbf{A}, \mathbf{A}')$ of eqs. (22) and (23).
3. DMO is presently run by applying a fixed step size Δs. However, considerable improvements are possible by applying a variable step size and automatically resolving avoided crossings detected with the help of overlap matrix and characteristic assignment amplitude.

DMO is generally applicable to properties of the reaction complex that depend on s. As an example, the ordering of orbitals and energy eigenstates along the reaction path has been discussed. Additional applications are possible when a generalized reaction path vector **u** is introduced. In the case that **u** represents the change in mass when converting one isotopomer into the other, the vibrational modes of the two isotopomers can be correlated correctly with the help of DMO. This is a special case of the more general problem of correlating the vibrational modes of two different molecules. As discussed in this work, the correlation problem can also be solved in this case using DMO.

Acknowledgment

All calculations were done on the Cray YMP/416 at the Nationellt Superdatorcentrum (NSC), Linköping, Sweden. The authors thank the NSC for a generous allotment of computer time.

References

1. W. H. Miller, N. C. Handy, and J. E. Adams, *J. Chem. Phys.*, **72,** 99 (1980).
2. For review articles, see: (a) W. H. Miller, *NATO ASI Ser. C*, **267,** 347 (1989); (b) S. C. Tucker and D. G. Truhlar, *NATO ASI Ser. C*, **267,** 291 (1989); (c) D. G. Truhlar and M. S. Gordon, *Science*, **249,** 491 (1990).
3. S. Kato and K. Morokuma, *J. Chem. Phys.*, **73,** 3900 (1980).

4. M. Page and J. W. J. McIver, *J. Chem. Phys.*, **88,** 922 (1988).
5. T. Taketsugu and M. S. Gordon, *J. Chem. Phys.*, **104,** 2834 (1996).
6. S. Kato, H. Kato, and K. Fukui, *J. Am. Chem. Soc.*, **99,** 684 (1977).
7. K. Yamashita, T. Yambe, and K. Fukui, *Chem. Phys. Lett.*, **84,** 123 (1981).
8. K. Morokuma and S. Kato, In: *Potential Energy Surfaces and Dynamic Calculations*, D. G. Truhlar, Ed., Plenum, New York, 1981, p. 243.
9. D. G. Truhlar, F. B. Brown, R. Steckler, D. C. Clar, Ed., *The Theory of Chemical Reaction Dynamics*, Reidel, Dordrecht, 1986, p. 285.
10. D. C. Fang and X. Y. Fu, Int. *J. Quant. Chem.*, **49,** 3 (1994).
11. J. A. Boatz and M. S. Gordon, *J. Phys. Chem.*, **93,** 5774 (1989).
12. Z. Konkoli and D. Cremer, *J. Phys. Chem. A*, **101**, 1742 (1997).
13. G. A. Natanson, *Mol. Phys.*, **46,** 481 (1982).
14. G. A. Natanson, B. C. Garrett, T. N. Truong, T. Joseph, and D. G. Truhlar, *J. Chem. Phys.*, **94,** 7875 (1991).
15. G. A. Natanson, *Chem. Phys. Lett.*, **178,** 49 (1991).
16. Z. Konkoli and D. Cremer, ADIA, A FORTRAN Program for the Adiabatic Mode Analysis and Unified Reaction Path Analysis, University of Göteborg, Göteborg, Sweden, 1996.
17. E. Kraka, J. Gauss, F. Reichel, L. Olsson, H. Zhi, Z. Konkoli, and D. Cremer, *COLOGNE96*, University of Göteborg, Göteborg, Sweden, 1996.
18. M. J. Rabinowitz, J. W. Sutherland, P. M. Patterson, and B. R. Klemm, *J. Phys. Chem.*, **95,** 674 (1991).
19. H. J. Baeck, K. S. Shin, H. Yang, Z. Qin, V. Lissianski, and W. C. J. Gardiner, *J. Phys. Chem.*, **99,** 15925 (1995).
20. V. D. Knyazev, A. Bencsura, S. I. Stoliarov, and I. R. Slagle, *J. Phys. Chem.*, **100,** 11346 (1996).
21. K. Yamashita and T. Yamabe, *Int. J. Quant. Chem.* (*Symp.*), **17,** 177 (1983).
22. G. C. Schatz, A. F. Wagner, and T. H. J. Dunning, *J. Phys. Chem.*, **88,** 221 (1984).
23. R. Steckler, K. J. Dykema, F. B. Brown, G. C. Hancock, D. G. Truhlar, and T. Valencich, *J. Chem. Phys.*, **87,** 7024 (1987).
24. T. Joseph, R. Steckler, and D. G. Truhlar, *J. Chem. Phys.*, **87,** 7036 (1987).
25. B. C. Garrett, M. J. Redmon, R. Steckler, D. G. Truhlar, K. K. Baldridge, D. Bartol, M. W. Schmidt, and M. S. Gordon, *J. Phys. Chem.*, **92,** 1476 (1988).
26. K. K. Baldridge, M. S. Gordon, R. Steckler, and D. G. Truhlar, *J. Phys. Chem.*, **93,** 5107 (1989).
27. D. H. Lu and D. G. Truhlar, *J. Chem. Phys.*, **99,** 2723 (1993).
28. T. N. Truong, *J. Chem. Phys.*, **100,** 8014 (1994).
29. C. F. Jackels, Z. Gu, and D. G. Truhlar, *J. Chem. Phys.*, **102,** 3188 (1995).
30. (a) C. Gonzales and B. H. Schlegel, *J. Phys. Chem.*, **94,** 5523 (1990); (b) C. Gonzales and B. H. Schlegel, *J. Chem. Phys.*, **90,** 2154 (1989).